Acta Biomaterialia 9 (2013) 6544–6552

Contents lists available at SciVerse ScienceDirect

Acta Biomaterialia

journal homepage: www.elsevier.com/locate/actabiomat

# Tyrosine-derived polycarbonate-silica xerogel nanocomposites for controlled drug delivery

M.C. Costache [a], A.D. Vaughan [b], H. Qu [c], P. Ducheyne [c], D.I. Devore [b,*]

[a] New Jersey Center for Biomaterials, Rutgers – The State University of New Jersey, Piscataway, NJ 08854, USA
[b] US Army Institute of Surgical Research, 3698 Chambers Pass, Fort Sam Houston, TX 78234, USA
[c] Center for Bioactive Materials and Tissue Engineering, Department of Bioengineering, University of Pennsylvania, Philadelphia, PA 19104, USA

ARTICLE INFO

*Article history:*
Received 24 May 2012
Received in revised form 14 January 2013
Accepted 29 January 2013
Available online 5 February 2013

*Keywords:*
Nanocomposites
Silica xerogel
Tyrosine-derived co-polymers
Mechanical properties
Controlled drug release

ABSTRACT

Biodegradable polymer–ceramic composites offer significant potential advantages in biomedical applications where the properties of either polymers or ceramics alone are insufficient to meet performance requirements. Here we demonstrate the highly tunable mechanical and controlled drug delivery properties accessible with novel biodegradable nanocomposites prepared by non-covalent binding of silica xerogels and co-polymers of tyrosine–poly(ethylene glycol)-derived poly(ether carbonate). The Young's moduli of the nanocomposites exceed by factors of 5–20 times those of the co-polymers or of composites made with micron scale silica particles. Increasing the fraction of xerogel in the nanocomposites increases the glass transition temperature and the mechanical strength, but decreases the equilibrium water content, which are all indicative of strong non-covalent interfacial interactions between the co-polymers and the silica nanoparticles. Sustained, tunable controlled release of both hydrophilic and hydrophobic therapeutic agents from the nanocomposites is demonstrated with two clinically significant drugs, rifampicin and bupivacaine. Bupivacaine exhibits an initial small burst release followed by slow release over the 7 day test period. Rifampicin release fits the diffusion-controlled Higuchi model and the amount released exceeds the dosage required for treatment of clinically challenging infections. These nanocomposites are thus attractive biomaterials for applications such as wound dressings, tissue engineering substrates and stents.

Published by Elsevier Ltd. on behalf of Acta Materialia Inc.

## 1. Introduction

There is an enormous unmet need for biomaterials that can address the many challenging requirements for mechanical, physicochemical, pharmacological and biological functionality in medical device applications [1–3]. In particular, biomaterials must be capable of addressing a wide range of mechanical properties from soft, viscoelastic topical wound dressings [4] to strong, elastic nerve guides [5,6] and cardiovascular stents [7–9], and further to hard, rigid bone tissue regeneration scaffolds [10,11]. Mechanical properties are increasingly recognized to have profound effects on the regulation of critical underlying biological tissue responses [12,13]. For most medical device applications the biomaterials must also be biocompatible, biodegradable and capable of controlled delivery of bioactive or therapeutic agents as needed for wound healing, tissue regeneration and control of pain, inflammation and infection [14–16].

Biocompatible composite materials that combine the processability and viscoelasticity of biodegradable organic polymers with the mechanical strength of biodegradable ceramic fillers offer significant potential to meet these biomaterial performance requirements when, as is often the case, the properties of polymers or ceramics alone are inadequate [17,18]. High mechanical strength can be imparted to composites through effective stress transfer between a continuous polymer matrix and the embedded inorganic particles. This requires effective interfacial bonding, either physical or covalent, between the ceramic and polymeric components [19]. The interfacial properties of polymer–inorganic composites also exert a strong influence on gas permeability, water uptake, drug release kinetics and cellular responses [20–24]. Both the physical and chemical properties of biomaterials can strongly affect the performance of and biological responses to drug delivery devices, wound dressings and tissue engineering scaffolds [12,13]. When biodegradable polymers are used to form the composites the biodegradation rates are significantly altered by the inorganic components, their concentration in the matrix and whether they are physically or covalently bonded to the organic polymer components [25,26].

A variety of non-degradable and biodegradable polymer–inorganic composites and nanocomposites have been studied, including polydimethylsiloxane or poly(methyl methacrylate)

* Corresponding author. Tel.: +1 210 539 9792; fax: +1 210 539 3877.
*E-mail address:* david.devore@us.army.mil (D.I. Devore).

1742-7061/$ - see front matter Published by Elsevier Ltd. on behalf of Acta Materialia Inc.
http://dx.doi.org/10.1016/j.actbio.2013.01.034

# Report Documentation Page

*Form Approved*
*OMB No. 0704-0188*



| 1. REPORT DATE | 2. REPORT TYPE | 3. DATES COVERED |
|---|---|---|
| **01 MAY 2013** | **N/A** | **-** |

| 4. TITLE AND SUBTITLE | 5a. CONTRACT NUMBER |
|---|---|
| **Tyrosine-Derived Polycarbonate-Silica Xerogel Nanocomposites for Controlled Drug Delivery.** | 5b. GRANT NUMBER |
| | 5c. PROGRAM ELEMENT NUMBER |
| 6. AUTHOR(S) | 5d. PROJECT NUMBER |
| **Costache M. C., Vaughan A. D., Qu H., Ducheyne P., Devore D. I.,** | 5e. TASK NUMBER |
| | 5f. WORK UNIT NUMBER |
| 7. PERFORMING ORGANIZATION NAME(S) AND ADDRESS(ES) | 8. PERFORMING ORGANIZATION REPORT NUMBER |
| **United States Army Institute of Surgical Research, JBSA Fort Sam Houston, TX** | |
| 9. SPONSORING/MONITORING AGENCY NAME(S) AND ADDRESS(ES) | 10. SPONSOR/MONITOR'S ACRONYM(S) |
| | 11. SPONSOR/MONITOR'S REPORT NUMBER(S) |

12. DISTRIBUTION/AVAILABILITY STATEMENT
**Approved for public release, distribution unlimited**

13. SUPPLEMENTARY NOTES

14. ABSTRACT

15. SUBJECT TERMS

| 16. SECURITY CLASSIFICATION OF: | | | 17. LIMITATION OF ABSTRACT | 18. NUMBER OF PAGES | 19a. NAME OF RESPONSIBLE PERSON |
|---|---|---|---|---|---|
| a. REPORT | b. ABSTRACT | c. THIS PAGE | | | |
| **unclassified** | **unclassified** | **unclassified** | **UU** | **9** | |

combined with silicates [27], poly(vinyl alcohol) (PVA) –montmorillonite clay [28], poly(ε-caprolactone) and tetraethoxysilane (TEOS) [24], polycaprolactone–graphene [29], and poly(lactide-co-glycolides) with hydroxyapatite, bioactive glass or calcium phosphates [26]. Most of these composites were made with bioactive ceramics to promote bone regeneration and only a few composites have been evaluated for controlled release of other therapeutics, such as aspirin [22] or the antibiotic ceftazidime [4].

Herein the focus is on the unique mechanical strength and controlled drug delivery properties of a novel family of biocompatible, biodegradable polymer–ceramic composites that has the potential to meet a very broad range of medical device requirements The composites are composed of silica xerogel ceramics [30,31] and co-polymers of tyrosine–poly(ethylene glycol)-derived poly(ether carbonate) [32,33]. Each of these components has been shown to be resorbable, non-cytotoxic and non-inflammatory in extensive in vitro and in vivo studies [33,34]. We compare the physical and mechanical properties of the composites as a function of co-polymer composition and the size of the ceramics, from the micron (microcomposites) to the nano (nanocomposites) scale. We also demonstrate their controlled drug release properties with two clinically important therapeutic agents, the antibiotic rifampicin and local anesthetic bupivacaine. These therapeutics were selected within the context of one potential application of the nanocomposites as wound dressings for treating infections [35] and pain [36]. More generally, rifampicin and bupivacaine span a range of hydrophobic to hydrophilic properties that strongly affect drug binding and delivery [37–39] and thus they also serve as models for assessing any drug–composite compatibility limitations for controlled delivery of other therapeutic agents that may be incorporated for various medical device applications.

## 2. Materials and methods

### 2.1. Materials

Tetraethoxysilane (TEOS) was obtained from Strem Chemicals (Newburyport, MA). Pyridine 99% was from Acros (Morris Plains, NJ). Poly(ethylene glycol), molecular weight 1000 Da (PEG1K) and bis(trichloromethyl)carbonate (triphosgene) were obtained from Fluka (Milwaukee, WI). Methylene chloride HPLC grade and methanol HPLC grade were obtained from Fisher Scientific (Morris Plains, NJ). Tetrahydrofuran (THF) was obtained from EMD (Gibbstown, NJ). 2-Propanol, bupivacaine hydrochloride, rifampicin, Dulbecco's phosphate-buffered saline, acetonitrile HPLC grade and water containing 0.1 vol.% trifluoroacetic acid were obtained from Sigma Aldrich (Milwaukee, WI). The tyrosine-derived poly(ether carbonate) co-polymers were prepared in the laboratory of Prof. Joachim Kohn (New Jersey Center for Biomaterials, Rutgers University, Piscataway, NJ).

### 2.2. Methods

#### 2.2.1. Co-polymer synthesis and characterization

The poly(ether carbonate) co-polymers used throughout this study were composed of monomers of desaminotyrosyl tyrosine ethyl ester (DTE) or octyl ester (DTO) and poly(ethylene glycol) (PEG) of molecular weight 1000 Da (Fig. 1). We refer to these as poly(DTE-co-10%PEG1k carbonate), abbreviated as E10, and poly (DTO-10%PEG1k carbonate), abbreviated as O10. The co-polymers were synthesized using a room temperature reaction of the DTO or DTE monomer and PEG1K with triphosgene in methylene chloride, quenching with THF solution and then recovering the co-polymer by solvent precipitation, as described in detail in the literature [32]. (Note that phosgenes are extremely toxic and must be used with extreme care in suitable hoods.) The co-polymer compositions, illustrated in Fig. 1, were confirmed by $^1$H nuclear magnetic resonance (DMSO-$d_6$, Varian VNMRS 400 MHz spectrometer) and Fourier transform infrared spectroscopy (Thermo Nicolet Avatar 380 spectrometer) using established chemical shift and absorption peak assignments [32]. The co-polymer number average ($M_n$) and weight average ($M_w$) molecular weights were determined by gel permeation chromatography (Waters Corp. 515 HPLC pump, 717 autosampler, 410 RI detector, and Empower 2 software) with 103 and 105 Å gel columns (Polymer Laboratories/Agilent, Santa Clara, CA) in series, with a THF mobile phase flow rate of 1 ml min$^{-1}$ and calibration based on polystyrene standards (Polymer Laboratories/Agilent).

#### 2.2.2. Xerogel micron scale particle synthesis

Silica xerogels were prepared at room temperature via a one-step acid catalyzed sol–gel process using tetraethoxysilane (TEOS) at a water:TEOS molar ratio of 10:1 [31]. Briefly, 1.0 M HCl was added to a mixture of water and TEOS at a 10:1 molar ratio to a final pH of 2.2. A clear sol formed after vigorous stirring for 20 min. The sol was cast into cylindrical polystyrene vials that were sealed and the sol allowed to gel and age at 37 °C for 2 days. Subsequently the vials were opened and the gels were allowed to dry in an oven at 37 °C for 3–4 days until the gel weight became constant. The silica gel was dried, crushed into granules, sieved using nylon meshes and sorted by particle size. Gas ($N_2$) adsorption/BET analysis (Autosorb-1, Quantachrome, Boynton Beach, FL) was used to determine the surface area, pore size and pore volume of xerogels that were first dried and outgassed at 50 °C for 20 h. Bupivacaine-containing xerogel microparticles were prepared by dissolving the drug in methanol and adding this directly to the acid catalyzed sol.

#### 2.2.3. Micron scale particle composite fabrication

Microcomposites were prepared with micron scale xerogel particles via solution blending as described previously [40]. For a typical 500 mg sample of microcomposite 350 mg E10 co-polymer was dissolved in 7 ml THF and 150 mg dry xerogel with the desired particle size was vigorously mixed in for 2 min. The slurry was then poured into a PTFE mold and the solvent evaporated over 48 h to yield a uniform film. The resulting film was dried under nitrogen flow for 24 h and in a vacuum oven at 50 °C for 24 h. The microcomposites were abbreviated as, for example, E10/M30, meaning a matrix of co-polymer E10 containing 30 wt.% silica xerogel microparticles (M).

#### 2.2.4. Nanocomposite synthesis and morphology

Nanocomposites were prepared in situ by first adding 1 ml deionized water to between 1.2 and 2 ml TEOS to obtain water: TEOS molar ratios *R* of 6–10, and catalyzing the hydrolysis reaction by addition of $7 \times 10^{-3}$ equivalents of HCl using 0.5 M HCl solution. The reaction mixture was stirred at room temperature for 16 h to allow complete TEOS hydrolysis without allowing the silica polycondensation reaction to reach the gel point. The silica sol was then mixed with 10% solutions of co-polymer in glacial acetic acid using increasing amounts of silica sol to obtain theoretical weight ratios of 0.5, 1, 3, 5, 10, 25, 30 and 50 wt.% $SiO_2$:co-polymer in the final nanocomposites. When the silica sols were added to the co-polymer solutions the resultant solutions remained transparent with no macroscopic phase separation or precipitation observed. The nanocomposite solutions were stirred for 5 min, poured into Teflon Petri dishes, dried under a nitrogen flow overnight, and then placed in a vacuum oven at 40 °C for a total of 96 h. Drug-loaded nanocomposites were prepared by stirring the prehydrolized TEOS solution with the co-polymer solution for 1 min, adding appropriate volumes of 2 mg ml$^{-1}$ bupivacaine or rifampicin in methanol, and proceeding as above. The nanocomposites were abbreviated

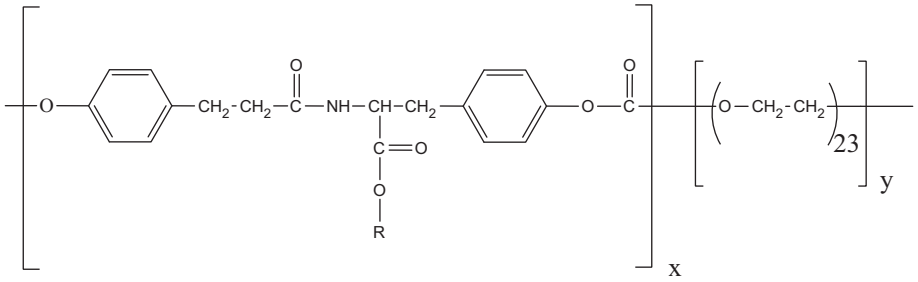

**Fig. 1.** Tyrosine–PEG-derived poly(ether carbonate) structure. Adjustable parameters are *x*, the mole fraction of the desaminotyrosyl tyrosine-derived monomer (DTR) (*x* is fixed at 90% in this study), and *y*, the mole fraction of PEG (*y* is fixed at 10% in this study), *R*, the pendent alkyl chain length (i.e. the monomer is "DTE" when the pendent group is ethyl, or "DTO" when it is octyl). The PEG molecular weight is fixed at 1000 daltons (DP = 23) in this study.

as, for example, E10/N30, meaning an E10 co-polymer nanocomposite (N) with 30 wt.% silica xerogel.

For transmission electron microscopy (TEM) nanocomposite films were embedded in low viscosity epoxy resin and cut into 50 nm thick samples using an ultramicrotome equipped with a diamond knife. The thin sections were transferred to carbon-coated copper grids (200 mesh) and imaged in a JEOL 100CX TEM operated at an accelerating voltage of 100 keV.

### 2.2.5. Thermal properties

The glass transition temperature ($T_g$) was determined by differential scanning calorimetry (2910 Modulated DSC, TA Instruments) on 10–15 mg samples. Specimens sealed in aluminum pans were subjected to a heat–cool–reheat program from −50 to 150 °C at a heating rate of 10 °C $min^{-1}$. The $T_g$ values were taken as the inflection points in the second heating scans of the DSC temperature program.

### 2.2.6. Tensile properties

The tensile properties of co-polymer and composite films ($30 \times 5 \times 0.20$ mm) were tested according to ASTM Standard D882-91 [41] in a Sintech 5/D tensile tester. Measurements were done in the dry state at room temperature. The Young's modulus, elongation (strain) and tensile strength data were averaged over 3–4 replicates. The initial grip speed was 2 mm $min^{-1}$ allowing reliable measurement of the elastic modulus. The yield point was calculated based on the zero slope criterion.

### 2.2.7. Equilibrium water uptake

Rectangular 200 μm thick, 60 mg samples of polymer and composites were immersed in phosphate-buffered saline (PBS) at 37 °C without shaking. At 30 min intervals samples were removed from the buffer, dried on a paper towel and weighed. The equilibrium water uptake (EWC) was calculated as the weight gain during incubation divided by the dry weight, $EWC = (W_{wet} - W_{dry})/W_{dry}$, and was taken as the point at which two consecutive time point samples had the same mass. Samples were run in triplicate.

### 2.2.8. In vitro degradation

Rectangular 200 μm thick, 60 mg samples were incubated in 20 ml PBS, pH 7.4 and 37 °C, and mixed at 100 r.p.m. The buffer was replaced every 2 days to maintain sink conditions and the mass loss was followed for 90 days. For each nanocomposite formulation (0.5, 1, 3, 5, 10, 25, 30 and 50 wt.% silica loading) and the co-polymer alone samples were removed from the buffer at selected time intervals, rinsed with DI water, freeze-dried and weighed. The mass loss was calculated as weight loss during incubation divided by the initial sample weight.

### 2.2.9. In vitro drug release and antimicrobial activity

The release rates of the local anesthetic bupivacaine from microcomposite and nanocomposite films were measured for up to 7 days using 30 mg samples incubated in 6 ml PBS at 37 °C in a Julabo SW2 water bath shaker at 100 r.p.m. The incubation medium was completely withdrawn at specified time intervals and replaced with 6 ml fresh buffer. The withdrawn samples were diluted 50:50 vol.% with acetonitrile and analyzed by high performance liquid chromatography (HPLC), as previously reported [40]. All experiments were performed in triplicate. Method validity was established from the specificity, linearity and accuracy according to International Conference on Harmonization (ICH) guidelines [42].

The antimicrobial activity of rifampicin and rifampicin-containing nanocomposites were determined against *Staphylococcus aureus* UAMS-1 (ATCC 49230), a clinical osteomyelitis strain, using a slightly modified Kirby–Bauer zone of inhibition (ZOI) method [43,44]. Frozen *S. aureus* UAMS-1 stock was thawed and diluted in 4 ml Mueller–Hinton II broth (cation-adjusted) (MHBII) to a density of 1 McFarland unit (~0.25 AU), then used to streak a lawn of bacteria onto Mueller–Hinton agar plates. Three circular 6 mm diameter discs of each nanocomposite were placed on the agar plates equidistant from each other and midway between the center and edge of the plate. The plates were incubated overnight at 37 °C, and the circular ZOI (absence of bacterial colonization, which was readily distinguished by visual inspection) measured with an electronic caliper.

## 3. Results

### 3.1. Compositions and morphologies of micron scale particle composites and nanocomposites

We successfully synthesized microcomposites and nanocomposites using three polymer matrices, poly(DTE-co-10%PEG1kcarbonate) (E10) and two different molecular versions of poly(DTO-co-10%PEG1kcarbonate) (O10 and O10′) (Table 1).

In the microcomposites the ground silica xerogel microparticles synthesized by the sol–gel process had random, jagged shapes and gas adsorption measurements gave the surface area and porosity values for the micron scale R10 silica xerogel particles of 362 $m^2$ $g^{-1}$ and 0.044 $cm^3$ $g^{-1}$, respectively. When loaded with 100 mg g bupivacaine the resultant xerogel microparticles had a

**Table 1**
Molecular weights of poly(DTE-PEG1k carbonate) and poly(DTO-PEG1k carbonate) co-polymers used to prepare the microcomposites and nanocomposites.

| Co-polymer | Abbreviation | $M_n$ (kDa) | $M_w$ (kDa) |
|---|---|---|---|
| Poly(DTE-10%PEG1k carbonate) | E10 | 93 | 156 |
| Poly(DTE-10%PEG1k carbonate) | O10 | 81 | 160 |
| Poly(DTE-10%PEG1k carbonate) | O10′ | 69 | 100 |

surface area of 0.1 $m^2 g^{-1}$ and a porosity of 0.005 $cm^3 g^{-1}$, indicative of the loaded drug filling up the pores of the silica microparticles and limiting gas adsorption. When the micron scale silica particles were mixed into the polymer matrices the resultant microcomposite films were somewhat opaque and light microscopic examinations revealed randomly dispersed microparticles throughout the polymer matrix. The xerogel microparticles in the microcomposites retain their jagged shape and drug loading had no apparent effect on microparticle distribution.

In contrast to the microcomposites, the nanocomposite films were transparent (Fig. 2), which is indicative of dispersion of the sub-micron particle size silica. After burning off the co-polymer in the nanocomposite at 700 °C the residual silica maintained the original shape of the film sample, which is further indicative of uniform dispersion of the silica throughout the nanocomposite matrix. The observed shrinking of the film was expected given that only 25% of the mass remained after burning off the co-polymer. The TEM micrographs of nanocomposites containing 3% silica xerogel (E10/N3) and 10% silica xerogel (E10/N10) have polymer-rich domains (lighter regions) and silica-rich domains (darker regions) with domain (or, phase) sizes of about 5–50 nm and no evidence of discreet micron scale particle formation (Fig. 3). As the silica content was increased the silica phase distribution in the nanocomposites remained uniform and continuous. When the drug bupivacaine or rifampicin was included in the formulations, the nanocomposites remained optically transparent. Rifampicin has a deep red color that was imparted to the nanocomposites, and visual inspection and light microscopy of these revealed a constant red color density indicative of a macroscopically uniform drug distribution throughout the nanocomposite. We did not attempt to measure the relative drug distributions in the nanocomposite silica and polymer phases.

### 3.2. Elastic mechanical properties

The Young's moduli of the composites were significantly greater than those of the co-polymers alone and increased with decreasing xerogel particle size. In fact, for the co-polymer poly(DTE-10%PEG1k)carbonate (E10) alone the modulus was 167 MPa, and at a fixed 30 wt.% xerogel content in E10 the microcomposite modulus increased from 430 MPa for the largest particle size range (70–105 μm) to 664 MPa for the smallest particle size range (10–20 μm), and the nanocomposite at this same 30 wt.% xerogel concentration had a modulus of 920 MPa, more than five times that of the co-polymer alone (Fig. 4).

The mechanical properties of the nanocomposites are strongly dependent on both the silica content, as illustrated by the stress–strain behavior of the poly(DTE-10%PEG1k)carbonate (E10) nanocomposites (Fig. 5). The Young's moduli for the E10 nanocomposites increased from 167 MPa for the E10 co-polymer alone to 384 MPa for the E10/N5 (5 wt.% silica) nanocomposite, and further increased to 768 MPa for the E10/N25 (25 wt.% silica) nanocomposite (Fig. 6). While the ultimate tensile strengths of the E10-based nanocomposites did not vary much over the range 0–25% silica, the elongations at fracture for these nanocomposites decreased with increasing silica content from 1230% for the E10 co-polymer alone to 12% for the E10/N25 nanocomposite at 25 wt.% silica (Fig. 6). Similar effects of silica content were seen with the poly(-DTO-10%PEG1k)carbonate (O10) nanocomposites, but the ultimate tensile strength was relatively more strongly influenced by silica content, increasing from 14 MPa for the O10 co-polymer alone to 52 MPa for the O10/N10 nanocomposite (Fig. 7). Switching from the DTE tyrosine-derived monomer in the E10 co-polymer to the DTO monomer in the O10 co-polymer resulted in significant decreases in all of the mechanical strength parameters of the co-polymers and their nanocomposites. This is due to the inherent relative strengths of the DTE- and DTO-based co-polymers; the octyl ester chains disrupt interchain hydrogen bonding that reduces self-association of the co-polymers [32,33] but, as was the case for the DTE-based composites, increasing the ceramic content increased the modulus of the DTO-based composites.

The addition of drug to the nanocomposites affects the mechanical properties, as demonstrated by the increase in modulus, yield strength and ultimate tensile strength for the O10′/N10 nanocomposite (Fig. 8). When rifampicin was added at 5 wt.% the modulus increased from 3.0 MPa for the drug-free nanocomposite to 7.0 MPa, and when the rifampicin content was raised to 10 wt.% the modulus increased to 12 MPa and the ultimate and yield tensile strengths roughly doubled compared with the drug-free nanocomposite.

### 3.3. Glass transition temperature

For the microcomposites of poly(DTO-co-10%PEG1k) (O10) with between 25 and 75 wt.% xerogel we previously showed that the $T_g$ value was 4 °C, not significantly different from the 2 °C $T_g$ of the co-polymer alone [40]. For poly(DTE-co-10%PEG1k carbonate) (E10) microcomposites containing 30% silica xerogel particles ranging in size from 10 to 105 μm the $T_g$ values were in the range 38–39 °C, the same as that of the co-polymer alone (Fig. 9). These results are indicative of minimal perturbation of polymer chain motion by the micron scale silica particles and, hence, of weak interfacial interactions between the co-polymers and silica particles.

In contrast to the microcomposites, the $T_g$ values for the nanocomposites were strongly affected by the silica content. For example, for the nanocomposite E10/N30 containing 30% silica in poly(DTE-co-10%PEG1kcarbonate) the $T_g$ was 85 °C, which is 46 °C higher than that of the co-polymer or the E10 microcomposites (Fig. 9). Similarly, for the nanocomposite O10/N50 containing 50% silica in poly(DTO-co-10%PEG1k)carbonate the $T_g$ was 59 °C, while the O10 co-polymer alone had a $T_g$ of only 2 °C. This behavior is indicative of a significant interfacial interaction between the co-polymer chains and the silica xerogel that significantly restricted co-polymer chain segment mobility. While the compositions and reaction conditions for nanocomposite formation preclude covalent bonding between the co-polymer chains and the silica, the observed $T_g$ increase with increasing xerogel content is consistent with an increasing number of interfacial non-covalent binding interactions, including hydrogen bonding between silica-derived hydroxyl groups and the co-polymer PEG oxygens and amide nitrogens, previously been shown to play a critical role in the mechanical properties of the tyrosine-derived co-polymers [45].

### 3.4. Equilibrium water uptake

For the microcomposites we previously found that the equilibrium water content (EWC) decreased from 17% for co-polymer

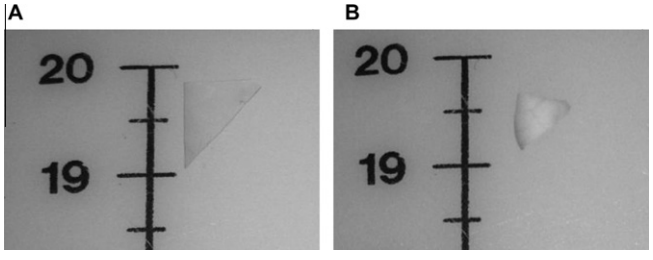


**Fig. 2.** Nanocomposite (O10/N25) film containing 25% silica xerogel. (A) Before and (B) after heating the film at 700 °C to burn off the poly(DTO-10%PEGcarbonate) co-polymer matrix. Scale units are inches.

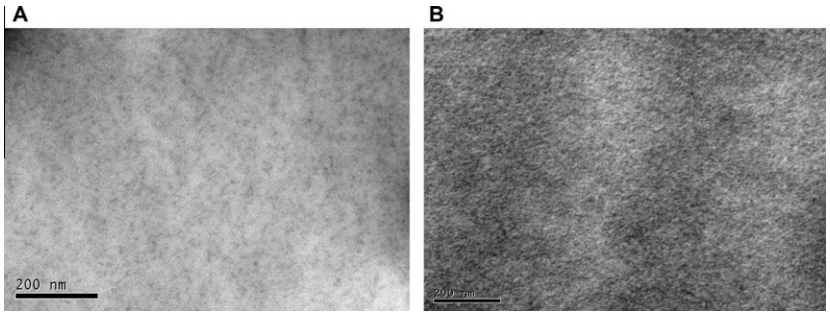


**Fig. 3.** TEM images of poly(DTE-10%PEGcarbonate) nanocomposites at (A) 3% and (B) 10% silica xerogel loading. Scale bar 200 nm.

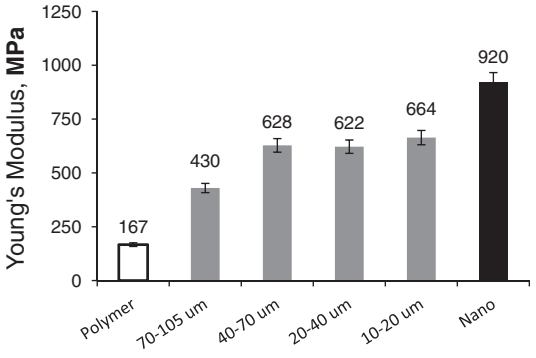


**Fig. 4.** Effect of particle size on the Young's modulus in the poly(DTE-co-10% PEG1k) carbonate (E10) microcomposite and nanocomposite formulations. The xerogel content was fixed at 30 wt.% in the poly(DTE-10%PEG1k)carbonate (E10) microcomposites and nanocomposite.

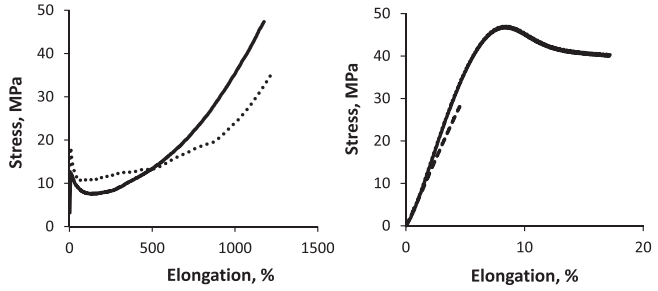


**Fig. 5.** The stress–elongation curves change with the fraction of silica in the poly(DTE-10%PEG1k)carbonate nanocomposites. (A) The solid line is poly(DTE-10%PEG1k)carbonate (E10), the dotted line is nanocomposite E10/N3. (B) The solid line is nanocomposite E10/N25, the dashed line is nanocomposite E10/N30.

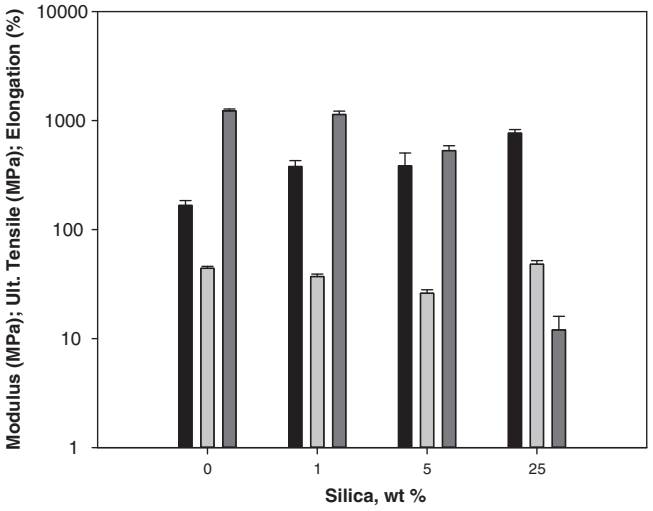


**Fig. 6.** Mechanical properties of nanocomposites of poly(DTE-co-10%PEG1k)carbonate (E10) as a function of silica content (wt.%). Black bars, Young's modulus (MPa); light grey bars, ultimate tensile strength (MPa); dark grey bars, elongation at break (%).

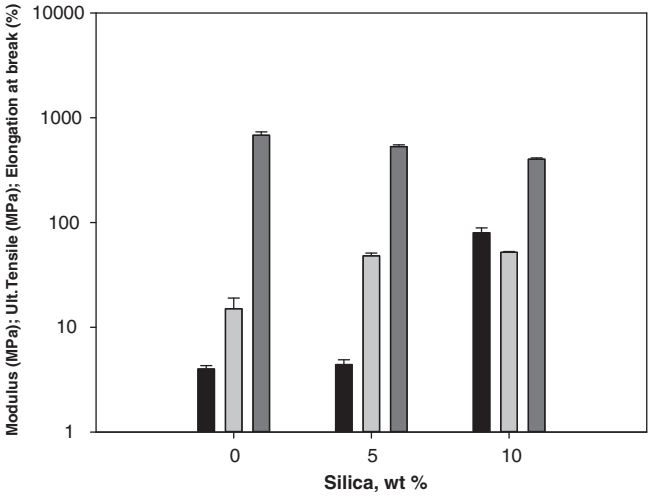


**Fig. 7.** Mechanical properties of nanocomposites of poly(DTO-co-10%PEG1k) as a function of silica content (wt.%). Black bars, Young's modulus (MPa); light grey bars, ultimate tensile strength (MPa); dark grey bars, elongation at break (%).

poly(DTO-10%PEG1k)carbonate (O10) alone to 11% as the microparticle silica content was increased to 75 wt.% [43]. This effect is seen with many but not all microparticle composites and depends upon the nature of the polymers and inorganic components, their particle volume fraction and any non-covalent or covalent bonding between the components [20,25,28,46,47]. As the silica loading in the poly(DTE-10%PEG1k)carbonate (E10) nanocomposites increased the equilibrium water content (EWC) decreased (Fig. 10). The poly(DTE-10%PEG1k)carbonate itself is a weakly absorbent hydrogel with an EWC of 18%. If the silica in the nanocomposites was inert and did not take up water or interact with the co-polymer chains then the amount of water uptake would be directly proportional to the mass fraction of co-polymer present. For example, for the nanocomposite of poly(DTE-10%PEG1k)carbonate containing 25% silica xerogel the mass fraction of co-polymer in the nanocomposite is 75% and that mass of co-polymer would by itself have an EWC of 13.5% (Fig. 10). The observed EWC for that

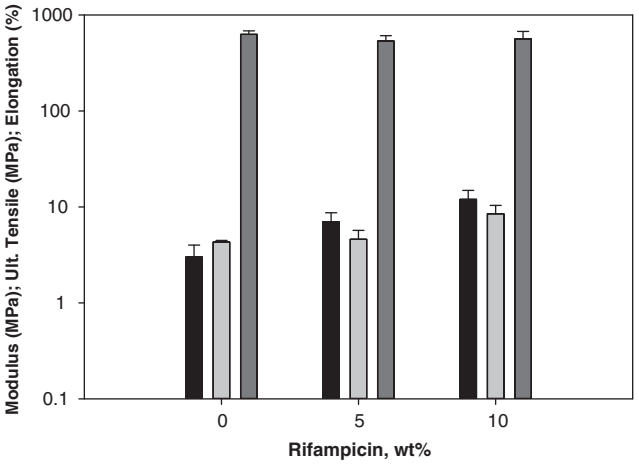


**Fig. 8.** The effect of rifampicin content on nanocomposite mechanical properties. Nanocomposites of poly(DTO-10%PEG1k)carbonate with 10 wt.% silica (O10′/N10) with 0, 5 and 10 wt.% rifampicin. Black bars, elastic modulus (MPa); dark grey bars, ultimate tensile strength (MPa); light grey bars, elongation at break, plotted as the fractional increase, $(L - L_o)/L_o$, rather than as a percentage.

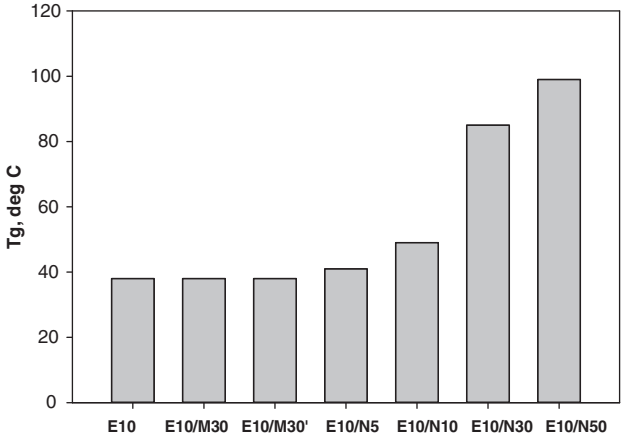


**Fig. 9.** Glass transition temperatures of composites as a function of silica xerogel particle size distributions. $T_g$ of co-polymer E10, microcomposites E10/M30 (with 10–20 μm silica microparticles) and E10/M30′ (with 70–100 μm silica microparticles), and nanocomposites E10/N5, E10/N10, E10/N30 and E10/N50.

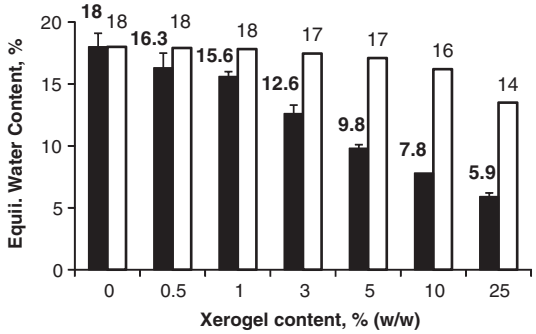


**Fig. 10.** Equilibrium water content for poly(DTE-10%PEG1k)carbonate nanocomposites are a function of silica xerogel concentration. Black bars, experimental EWC values, where EWC = $(W_{wet} - W_{dry})/W_{dry}$; white bars, calculated EWC values based on the assumption that only the mass of co-polymer present takes up water.

nanocomposite was only 5.9%, however, which further demonstrates a significant interfacial interaction between the silica and the co-polymer such that co-polymer chain mobility is greatly restricted and water uptake is thereby reduced. The water uptake for all E10 nanocomposite samples rose rapidly to their plateau values, the EWC, within 5 h. For both DTE- and DTO-derived co-polymers by themselves the EWC had previously been shown to increase rapidly with increasing PEG content, for example the water uptake of DTO-10%PEG is 17%, while for DTO-20%PEG it is 65% [32,40], and similar effects of PEG content on the EWC would be expected for the microcomposites and nanocomposites.

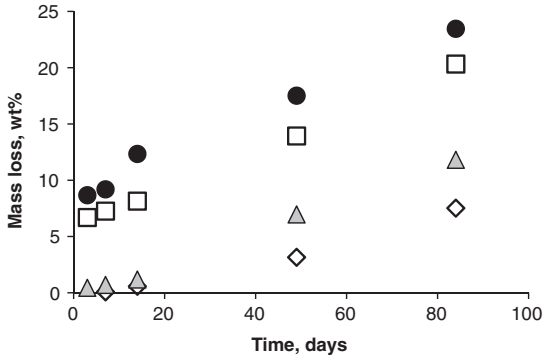


**Fig. 11.** Hydrolytic mass loss of poly(DTE-10%PEG1k)carbonate nanocomposites as a function of silica content. ◇, co-polymer E10; ▲, nanocomposite with 5% xerogel; □, nanocomposite with 25% xerogel; ○, nanocomposite with 50% xerogel.

### 3.5. Hydrolytic degradation and erosion

The mass loss of the poly(DTE-10%PEG1k)carbonate co-polymer by itself during incubation in buffer solution at 37 °C was negligible for 6 days and then increased slowly over several weeks (Fig. 11). The mass loss for the nanocomposites during incubation was significantly greater than that of the co-polymer alone at every time interval and increased with increasing silica xerogel concentration. The kinetics of nanocomposite degradation after the initial 24 h period were essentially linear with time, with a mass loss rate calculated from the slopes of the data in Fig. 9 of about 0.16 wt.% $day^{-1}$ independent of their silica weight fraction, while the mass loss rate of the co-polymer alone was only about 0.07 wt.% $day^{-1}$. We attribute the faster degradation rate of the nanocomposites to relatively rapid dissolution of the silica phase [30,40]. The water uptake and degradation rate of the composites could be increased by increasing the PEG content of the co-polymers and decreased by substituting the more hydrophobic DTO monomer for the DTE monomer [32,40].

### 3.6. Drug release and antimicrobial activity

The release kinetics of bupivacaine from the microcomposites and nanocomposites were obtained for the poly(DTO-10%PEG1k)carbonate co-polymer alone and at 50 wt.% silica (O10/M50 and O10/N50) at a fixed loading of 8 wt.% bupivacaine. The DTO co-polymers were used here rather than DTE because we had previously found that the more hydrophobic DTO co-polymers provided improved barrier control of water influx and drug efflux of the local anesthetics bupivacaine and mepivacaine from the microcomposites [40]. The co-polymer alone exhibited an initial very large burst release stage of 50% of the drug load in the first 24 h, followed by a second stage of relatively constant slow release (Fig. 12). In the O10/M50 microcomposite the drug was initially confined entirely within the nanopores of the xerogel particles and the co-polymer matrix acted as a barrier to further control water influx and drug efflux. The porosity of the micron scale xerogel particles and the hydrophobicity of the co-polymer matrix determine the drug release kinetics of the microcomposites [40],

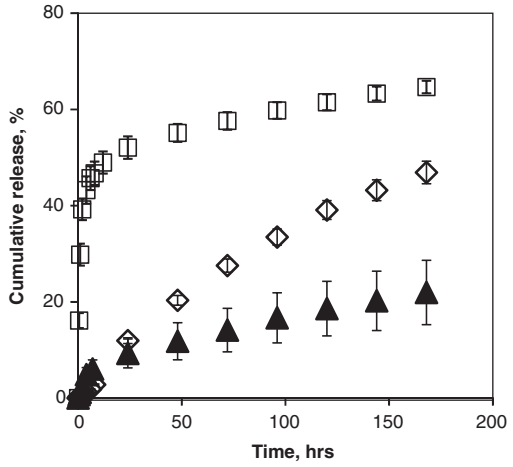


**Fig. 12.** Bupivacaine release from co-polymer, microcomposite and nanocomposite. □, copolymer poly(DTO-10%PEG1k)carbonate (O10); ◇, microcomposite (O10/M50), ▲, nanocomposite (O10/N50). The microcomposite and nanocomposite contain the same silica loading, 50 wt.%, with a fixed bupivacaine content of 8 wt.% for all of the samples.

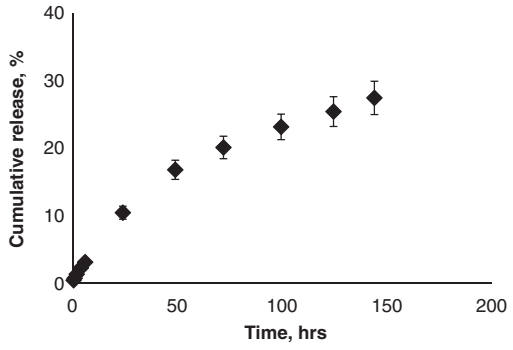


**Fig. 13.** Nanocomposite release of rifampicin. Rifampicin loading was 10 wt.% in the poly(DTO-10%PEG1k)carbonate/10% silica (O10/N10) nanocomposite.

which for O10/M50 is also two stage but slower than the co-polymer and essentially zero order over the first 72 h (Fig. 12). The O10/N50 nanocomposite also exhibits a two stage behavior but has a much reduced initial stage release of only 10% of the drug in the first 24 h and thereafter continues to release the drug at a rate comparable with that of the co-polymer.

The release rate of the antibiotic rifampicin from the O10/N10 nanocomposite with an initial loading of 10 wt.% rifampicin (Fig. 13) was again a two stage process, with about 10% of the rifampicin load rapidly released in the first 24 h stage followed by a slower second stage release rate. When the cumulative rifampicin release data are plotted as a function of $t^{1/2}$ they can be fitted to a single straight line (correlation coefficient 0.98), which is consistent with the Higuchi model for diffusion-controlled drug release [48]. The nanocomposites retained the antimicrobial activity of the incorporated rifampicin, as demonstrated by the ZOI of *S. aureus* UAMS-1 growth: 34.4 ± 0.8 mm for the rifampicin-containing nanocomposite O10/N10 with 10 wt.% drug loading and 44.7 ± 1.8 mm for free rifampicin at the same initial drug concentration.

## 4. Discussion

We were able to prepare microcomposites and nanocomposites of tyrosine–PEG-derived polyether carbonate co-polymers and silica xerogels by simple mixing processes. The microcomposites are slightly opaque due to the random distribution of the silica xerogel microparticles throughout the co-polymer matrix. In contrast, the nanocomposites were transparent and, based on the TEM micrographs, appeared as a two phase material with silica xerogel domains of about 5–50 nm homogeneously distributed throughout the co-polymer matrix.

To prepare drug-loaded xerogel microparticles for the microcomposites we started with a silica solution and the drug was uniformly distributed in the sol, as indicated by the absence of any turbidity. Under these conditions the drug molecules were uniformly entrapped as gelling progressed. In these studies drug loading in the microcomposites was limited to the microparticles, although it would also be possible to load drug into the co-polymer matrix [40]. In the absence of any drug the silica microparticle surface area (386 $m^2\ g^{-1}$) was the total surface area, including the surface area inside the particle pores. There was an enormous decrease in surface area of the microparticles to 0.1 $m^2\ g^{-1}$ when bupivacaine was added. The drug filled the pores, as reflected in the greatly reduced porosity of 0.005 $cm^3\ g^{-1}$, and, hence, in the presence of the drug only the outer sphere area was measured in gas adsorption experiments. In contrast, the nanocomposites were two phase materials and each of the phases had its own physical and chemical properties. At this time we do not have any experimental evidence regarding distribution of the drug in the two phases but, based on the chemical synthesis methodology of the nanocomposites, we assume a uniform distribution throughout.

The mechanical and glass transition properties of our microcomposites and nanocomposites depended on the size and the amount of silica xerogel present. For the microcomposites we found that the yield strengths and $T_g$ values of the co-polymers were not greatly affected by the incorporation of xerogel microparticles and, as previously shown [40], the equilibrium water uptake was only slightly decreased. The elongation at break of the co-polymers were, however, substantially reduced by incorporation of xerogel microparticles. Given that the yield strengths and $T_g$ values are measures of the motion of polymer chain segments, which is dependent on chain rigidity, cohesive energy density, polarity, molecular weight and crosslinking, these results are indicative of weak interfacial bonding between the microparticles and co-polymers but the microparticles act as physical barriers that restrict co-polymer chain mobility.

In the nanocomposites increasing the silica content increased the mechanical strength and $T_g$ while decreasing the equilibrium water content (EWC), all of which are indicative of a strong interfacial interaction between the co-polymer and silica phases. Addition of the drug rifampicin to the nanocomposite also resulted in an increase in the mechanical strength. Hydrogen bonding interfacial interactions between the large number of ethylene oxide units in the co-polymer backbone, the silica phase and any drug molecules present may act as physical crosslinkers and explain the reduced polymer chain mobility, reflected in the increased tensile properties and $T_g$. Rifampicin has a large number of alcohol, carbonyl, amine and ether groups that can participate in hydrogen bonding with the silica and PEG groups of the nanocomposite. Bupivacaine, in contrast, has only one secondary amine and one carbonyl group, so although we did not measure them we would anticipate a much lesser effect of bupivacaine or similar molecules on the mechanical properties of the nanocomposites. The mechanical properties required for specific medical devices vary considerably depending on the application. The required tensile strengths and elastic moduli for wound dressings range from about 1 to 24 MPa and from about 1 to 490 MPa, respectively [4]. Human Achilles tendon has a tensile stress and modulus of about 71 and 816 MPa, respectively [49]. Cortical bone has a longitudinal tensile yield strength and Young's modulus of about 78–151 MPa and

17–20 GPa, respectively, while the yield strength and modulus of trabecular bone are about 5–10 and 50–100 MPa, respectively [50]. As can be seen from the data in Figs. 6–8, the mechanical properties of the nanocomposites are within these limits with the exception of the modulus for cortical bone, which because of its great stiffness and lack of elongation has a very high modulus that is outside the range found with the composites tested here. For comparison, the tensile strength and modulus of poly(lactide-co-glycolide) (PLGA), one of the most thoroughly studied biodegradable co-polymers for bone regeneration and many other applications, are about 41–55 MPa and 1.4–2.8 GPa, respectively [26], while photo-crosslinked poly(ε-caprolactone fumarates) (PCLF), designed as nerve regeneration conduits, have tensile strengths and moduli of 0.48–7.1 and 0.87–138 MPa, respectively [6]. The nanocomposites have far greater strength than PCLF at comparable flexibility levels and greater flexibility than PLGA at a given strength level, enabling improvements for such potential applications of the nanocomposites as nerve conduits, wound dressings and sutures.

The $T_g$ behavior of our nanocomposites contrasts with similarly prepared nanocomposites based upon poly(ε-caprolactone) and TEOS-derived silica, where no significant increase in $T_g$ is observed with increased silica content in the nanocomposites [24]. The difference between the poly(ε-caprolactone) nanocomposites and the present poly(DTE-10%PEG1k)carbonate nanocomposites can be ascribed to the large number of PEG oxygen atoms present in our poly(DTE-10%PEG1k)carbonate co-polymers compared with poly(ε-caprolactone), which provides only a very limited number of ester group oxygen atoms for hydrogen bonding to the silica-derived hydroxyl groups, and, hence, there is no significant increase in interfacial hydrogen bonding as the silica nanoparticle content is increased in the poly(ε-caprolactone) nanocomposites.

Sustained controlled drug delivery was obtained with both the microcomposites and nanocomposites. We previously demonstrated that in the microcomposites the controlled release of bupivacaine can be tuned from burst to zero order kinetics by varying the co-polymer compositions and drug loading [40]. Here we have focused on the release of bupivacaine and rifampicin from the nanocomposites. These drugs were selected because they have very different physical properties that affect drug binding and delivery in vitro and in vivo, i.e. for rifampicin the octanol:water partition log$P$ = 2.7 and the polar surface area (PSA) is 220 (DrugBank website, http://www.drugbank.ca/) [51], which are typical of relatively hydrophobic compounds, while for the hydrophilic bupivacaine log$P$ = 0.30 [52] and PSA = 32.3[51]. The relatively small difference in hydrolytic degradation of the co-polymer and the nanocomposite over the first 24 h cannot explain the significant reduction in the initial release of bupivacaine from the nanocomposite. Rather, this difference is ascribed to differences in water influx and drug efflux from the samples, which are determined by the different physical state of the co-polymer chains. When no silica is present the drug-loaded co-polymer is in a rubbery state ($T_g$ = 2 °C). In contrast, the nanocomposites are in a glassy state, as evidenced by the higher $T_g$ of 59 °C for O10/N50. Therefore the co-polymer chain mobilities in the nanocomposites are more restricted and water uptake is reduced, which slows drug solubilization and diffusion out of the nanocomposite compared with the co-polymer. The silica phase in the nanocomposite may also impede efflux from the nanocomposites by binding the drugs and/or by acting as physical barriers to flow.

The similarity of the release profiles for rifampicin and bupivacaine from the nanocomposites reflects a balancing of the physical properties of the two drugs with the water uptake properties of the two nanocomposites: the O10/N50 nanocomposite presents a greater barrier to water uptake and, hence, limits efflux of the hydrophilic bupivacaine, while the greater water uptake of the O10/N10 nanocomposite enables efflux of the hydrophobic rifampicin. The amount of rifampicin released from the nanocomposite in the first 24 h was 0.06 mg ml$^{-1}$, which exceeds the minimum inhibitory concentration (MIC) for planktonic methicillin-resistant *S. aureus* (MRSA) infections [53] and for *Staphylococcus epidermidis* biofilms [54]. In our Kirby–Bauer ZOI test we found that the rifampicin released from the O10/N10 nanocomposite retained its antimicrobial activity against the clinically derived osteomyelits strain *S. aureus* UAMS1. Given that the cumulative rifampicin release rate into PBS from the nanocomposite in our controlled release study was only about 10% in the 24 h corresponding to the duration of the ZOI test the observed antimicrobial activity of the nanocomposite, which was comparable with that of the free rifampicin control, is indicative of the bacteria acting as attractive "sinks" that bind the drug and thereby drive its diffusion out of the nanocomposite.

## 5. Conclusions

By varying the silica loading and the co-polymer matrix compositions we have demonstrated that microcomposites and nanocomposites of silica xerogels and tyrosine–poly(ethylene glycol)-derived poly(ether carbonates) provide a remarkably broad and uniquely tunable range of mechanical and drug delivery properties under in vitro physiological conditions. The mechanical properties are superior to those of the poly(ether carbonate) co-polymer alone as well as to other well-known biodegradable co-polymers such as PLGA and they uniquely provide for tunable, controlled release of both hydrophilic and hydrophobic therapeutic agents. We have previously demonstrated that the activity of bupivacaine in our microcomposites is retained in vivo based upon a rat incisional pain model study [55]. These novel biomaterials therefore merit further study for such applications as implantable drug delivery depots, wound dressings, tissue engineering scaffolds and cardiovascular stents, where mechanical strength and controlled drug release properties are essential.

## Disclosures

We have no conflicts of interest.

## Acknowledgements

This work was supported in part by US Army contract no. W81XWH-07-1-0438. The US Army Medical Research Acquisition Activity, Fort Detrick, MD, was the awarding and administering acquisition office. The content of the manuscript does not necessarily reflect the position or the policy of the Government, and no official endorsement should be inferred. Support from the US Army Institute of Surgical Research and the New Jersey Center for Biomaterials, Rutgers University, is gratefully acknowledged. The authors thank Dr. Das Bolikal and Dr. Joachim Kohn of Rutgers University for their assistance.

## References

[1] Goldberg M, Langer R, Jia X. Nanostructured materials for applications in drug delivery and tissue engineering. J Biomater Sci Polym Ed 2007;18:241–68.
[2] Kohn J. New approaches to biomaterials design. Nat Mater 2004;3:745–7.
[3] Fisher OZ, Khademhosseini A, Langer R, Peppas NA. Bioinspired materials for controlling stem cell fate. Acc Chem Res 2010;43:419–28.
[4] Elsner JJ, Shefy-Peleg A, Zilberman M. Novel biodegradable composite wound dressings with controlled release of antibiotics: microstructure, mechanical and physical properties. J Biomed Mater Res B 2010;93:425–35.
[5] Subramanian A, Krishnan UM, Sethuraman S. Development of biomaterial scaffold for nerve tissue engineering: biomaterial mediated neural regeneration. J Biomed Sci 2009;16:108–29.

[6] Wang S, Yaszemski MJ, Knight AM, Gruetzmacher JA, Windebank AJ, Lu L. Photo-crosslinked poly(ε-caprolactone fumarate) networks for guided peripheral nerve regeneration: material properties and preliminary biological evaluations. Acta Biomater 2009;5:1531–42.
[7] Francolini I, Crisante F, Marinelli A, D'Ilario L, Piozzi A. Synthesis of biomimetic segmented polyurethanes as antifouling biomaterials. Acta Biomater 2012;8:549–58.
[8] Kohn J, Zeltinger J. Degradable, drug-eluting stents: a new frontier for the treatment of coronary artery disease. Expert Rev Med Devices 2005;2:667–84.
[9] Grabow N, Martin DP, Schmitz K-P, Sternberg K. Absorbable polymer stent technologies for vascular regeneration. J Chem Technol Biotechnol 2010;85:744–51.
[10] Hutmacher DW. Scaffolds in tissue engineering bone and cartilage. Biomaterials 2000;21:2529–43.
[11] Ramay HR, Zhang M. Preparation of porous hydroxyapatite scaffolds by combination of the gel-casting and polymer sponge methods. Biomaterials 2003;24:3293–302.
[12] Mitragotri S, Lahann J. Physical approaches to biomaterial design. Nat Mater 2009;8:15–23.
[13] Rehfeldt F, Engler AJ, Eckhardt A, Ahmed F, Discher DE. Cell responses to the mechanicochemical microenvironment – implications for regenerative medicine and drug delivery. Adv Drug Deliv Rev 2007;59:1329–39.
[14] Lee S-H, Shin H. Matrices and scaffolds for delivery of bioactive molecules in bone and cartilage tissue engineering. Adv Drug Deliv Rev 2007;59:339–59.
[15] Boateng JS, Matthews KH, Stevens HNE, Eccleston GM. Wound healing dressings and drug delivery systems: a review. J Pharm Sci 2008;97:2892–923.
[16] Moioli EK, Clark PA, Xin X, Lal S, Mao JJ. Matrices and scaffolds for drug delivery in dental, oral and craniofacial tissue engineering. Adv Drug Deliv Rev 2007;59:308–24.
[17] Ruiz-Hitzky E, Darder M, Aranda P, Ariga K. Advances in biomimetic and nanostructured biohybrid materials. Adv Mater 2010;22:323–36.
[18] Zhao R, Torley P, Halley PJ. Emerging biodegradable materials: starch- and protein-based bio-nanocomposites. J Mater Sci 2008;43:3058–71.
[19] McCrum NG, Buckley CP, Bucknall CB. Principles of polymer engineering. 2nd ed. Oxford: Oxford University Press; 1999.
[20] Cornelius CJ, Marand E. Composite silica-polyimide composite membranes: gas transport properties. J Membr Sci 2002;202:97–118.
[21] Rhee SH. Preparation of a bioactive poly(methyl methacrylate)/silica nanocomposite. J Am Ceram Soc 2002;85:1318–20.
[22] Lin M, Wang H, Meng S, Zhong W, Li Z, Cai R, et al. Structure and release behavior of PMMA/silica composite drug delivery system. J Pharm Sci 2007;96:1518–26.
[23] Lee EJ, Shin DS, Kim HE, Kim HW, Koh YH, Jang JH. Membrane of hybrid chitosan–silica xerogel for guided bone regeneration. Biomaterials 2009;30:743–50.
[24] Young SK, Gemeinhardt GC, Sherman JW, Storey RF, Mauritz KA, Schiraldi DA, et al. Covalent and non-covalently coupled polyester–inorganic composite materials. Polymer 2002;43:6101–14.
[25] Maquet V, Boccaccini AR, Pravata L, Notingher I, Jerome R. Preparation, characterization and in vitro degradation of bioresorbable and bioactive composites based on bioglass-filled polylactide foams. J Biomed Mater Res 2003;66A:335–46.
[26] Rezwan K, Chen QZ, Blaker JJ, Boccaccini AR. Biodegradable and bioactive porous polymer/inorganic composite scaffolds for bone tissue engineering. Biomaterials 2006;27:3413–31.
[27] Arcos D, Vallet-Regi M. Sol–gel silica-based biomaterials and bone tissue regeneration. Acta Biomater 2010;6:2874–88.
[28] Kokabi M, Sirousazar M, Hassan ZM. PVA–clay nanocomposite hydrogels for wound dressing. Eur Polym J 2007;43:773–81.
[29] Wan C, Chen B. Poly(Îμ-caprolactone)/graphene oxide biocomposites: mechanical properties and bioactivity. Biomed Mater 2011;6:055010. 1–8.
[30] Nicoll SB, Radin S, Santos EM, Tuan RS, Ducheyne P. In vitro release kinetics of biologically active transforming growth factor-[beta]1 from a novel porous glass carrier. Biomaterials 1997;18:853–9.
[31] Radin S, Ducheyne P, Kamplain T, Tan BH. Silica sol–gel for the controlled release of antibiotics. I. Synthesis, characterization, and in vitro release. J Biomed Mater Res 2001;57:313–20.
[32] Yu C, Kohn J. Tyrosine–PEG-derived polyether carbonates as new biomaterials. Part I: synthesis and evaluation. Biomaterials 1999;20:253–64.
[33] Bourke SL, Kohn J. Polymers derived from the amino acid L-tyrosine: polycarbonates, polyarylates and copolymers with poly(ethylene glycol). Adv Drug Deliv Rev 2003;55:447–66.
[34] Radin S, El Bassyouni G, Vresilovic EJ, Schepers E, Ducheyne P. In vivo tissue response to resorbable silica xerogels as controlled release materials. Biomaterials 2005;26:1043–52.
[35] Murray CK, Obremskey WT, Hsu JR, Andersen RC, et al. Prevention of infections associated with combat-related extremity injuries. J Trauma 2011;71(Suppl. 2):S235–7.
[36] Clark ME, Bair MJ, Buckenmaier CC, Gironda RJ, Walker RL. Pain and combat injuries in soldiers returning from Operations Enduring Freedom and Iraqi Freedom: implications for research and practice. J Rehabil Res Dev 2007;44:179–94.
[37] Stenberg P, Bergström CAS, Luthman K, Artursson P. Theoretical predictions of drug adsorption in drug discovery and development. Clin Pharmacokinet 2002;41:877–99.
[38] Lipinski CA, Lombardo F, Dominy BW, Feeney PJ. Experimental and computational approaches to estimate solubility and permeability in drug discovery and development settings. Adv Drug Deliv Rev 2001;46:3–26.
[39] Clark DE. What has polar surface area ever done for drug discovery? Future Med Chem 2011;3:469–84.
[40] Costache MC, Qu H, Ducheyne P, Devore DI. Polymer–xerogel composites for controlled release wound dressings. Biomaterials 2010;31:6336–43.
[41] ASTM. Standard D638–10, Standard test method for tensile properties of plastics. West Conshohocken, PA: ASTM International; 2003.
[42] Topic Q2B. Validation of analytical procedures: methodology. In: Proceedings of the international conference on harmonization (ICH), Rockville, MD. U.S: Food and Drug Adminstration; 1996.
[43] Percival SL, Bowler PG, Dolman J. Antimicrobial activity of silver containing dressings on wound microorganisms using an in vitro biofilm model. Int Wound J 2007;4:186–91.
[44] Bauer AW, Kirby WMM, Sherris JC, Turck M. Antibiotic susceptibility testing by a standardized single disc method. Am J Clin Pathol 1966;45:493–6.
[45] Jaffe M, Ophir Z, Collins G, Recber A, Yoo S-U, Rafalko JJ. Process–structure–property relationships of erodible polymeric biomaterials: II. Long range order in poly(desaminotyrosyl arylates). Polymer 2003;44:6033–42.
[46] Jian G, Liu C, Liu X, Chen Q, Zhang G, Yang M, et al. Network structure and compositional effects on tensile mechanical properties of hydrophobic association hydrogels with high mechanical strength. Polymer 2010;51:1507–15.
[47] Haraguchi K, Takehisa T. Nanocomposite hydrogels: a unique organic–inorganic network structure with extraordinary mechanical, optical and swelling/de-swelling properties. Adv Mater 2002;16:1120–3.
[48] Sinko PJ. Martin's physical pharmacy and pharmaceutical science. 5th ed. Baltimore, MD: Lippincott, Williams & Wilkins; 2006. pp. 327–329.
[49] Wren TAL, Yerby SA, Beaupre GS, Carter DR. Mechanical properties of the human Achilles tendon. Clin Biomech 2001;16:245–51.
[50] Porter JR, Ruckh TT, Popat KC. Bone tissue engineering: a review in bone biomimetics and drug delivery strategies. Biotechnol Prog 2009;25:1539–60.
[51] Knox C, Law V, Jewison T, Liu P, Ly S, et al. DrugBank 3.0: a comprehensive resource for "omics" research on drugs. Nucleic Acids Res 2011;39(Database issue):D1035–41.
[52] Strichartz GR, Sanchez V, Arthur GR, Chafetz R, Martin D. Fundamental properties of local anesthetics. II. Measured octanol:buffer partition coefficients and p$K_a$ values of clinically used drugs. Anesth Analg 1990;71:158–70.
[53] Salem AH, Elkhatib WF, Moreddin AM. Pharmacodynamic assessment of vancomycin–rifampicin combination against methicillin resistant *Staphylococcus aureus* biofilm: a parametric response surface analysis. J Pharm Pharmacol 2011;63:73–9.
[54] Dunne WM, Mason EO, Kaplan SL. Diffusion of rifampin and vancomycin through a *Staphylococcus epidermidis* bioflm. Antimicrob Agents Chemother 1993;37:2522–6.
[55] Qu H, Costache MC, Inan S, Cowan A, Devore D, Ducheyne P. Local, controlled delivery of analgesics in vivo from polymer–xerogel composites, submitted for publication.